Normal to abnormal behavior of PbSiO3 glass: a vibrational spectroscopy investigation under high-pressure

R.B. Pena, Thierry Deschamps, Alex Amato, Sylvie Le Floch, Paolo Pizani, C. Martinet

Normal to abnormal behavior of $PbSiO_3$ glass: a vibrational spectroscopy investigation under high-pressure

R.B. Pena[a,b,c]; T. Deschamps[a]; A. Amato[a]; S. Le Floch[a] ; P.S. Pizani[b,c]; C. Martinet[a]

[a] Institut Lumière Matière (ILM), UMR5306 Université Lyon 1 - CNRS, Université de Lyon 69622 Villeurbanne, France.

[b] Federal University of São Carlos, Physics Department, 13565 - 905 São Carlos, SP, Brazil.

[c] Department of Materials Engineering, Center for Research, Technology and Education in Vitreous Materials, Federal University of São Carlos, 13565-905, São Carlos, SP, Brazil.

Highlights (maximum 85 characters)

- Brillouin investigation of $PbSiO_3$ glass cold-densified at different maximum pressure (85 characters!)
- Densification induces anomaly in elastic modulus despite the low silica content (79 characteres!)
- The verified anomaly distinguishes from the elastic anomaly then absent in this glass (85 characters!)
- Abnormal decrease on longitudinal sound velocity whereas the density increases marginally. (85 characters!)

Abstract: High pressure may pave the way towards atypical phenomena and properties in glass science. Through compression, vitreous silica presents a well-established elastic anomaly (EA) and the scarcely investigated elastic modulus anomaly (EMA). In this paper, we highlight an EMA for the densified lead metasilicate ($PbSiO_3$) glass, despite its low silica content and lack of the classical EA. $PbSiO_3$ glass was densified in diamond anvil cell and Belt press apparatus and analyzed by Brillouin spectroscopy and, when applicable, spectroscopic ellipsometry. Elastic modulus anomaly is manifested by a decrease in the longitudinal sound velocity of the densified glass compared to the uncompressed glass and attributed to the low glass ability to undergo significant densification. Densification pathways in $PbSiO_3$ glass are discussed in light of in-situ Brillouin and Raman probes.

Keywords: *High-Pressure; Mechanical Properties; Elastic Anomaly; Brillouin Spectroscopy; Lead Metasilicate Glass.*

1. Introduction

Mechanical and acoustical studies carried out on some compositions of silicate glasses show an abnormal behavior of the elastic constants under pressure, so-called the elastic anomaly (EA). This anomaly was first identified on the elastic compressibility of a Pyrex glass with a high silica content [1] and then confirmed in vitreous silica [2] and several silicate glass compositions [3, 4]. These glasses display, under elastic compression, an abnormal behavior for bulk modulus, which first decreases and then follows a normal increasing behavior as a function of pressure [5], presenting a pressure minimum at about 1-3 GPa, with the minimum behavior and the accurate value depending on the glass composition [4]. The same non-monotonic trend also appears on the acoustic velocities, as probed by Brillouin spectroscopy [6, 7] and ultrasonic means [5].

While the aforementioned EA is established in the glass literature, a less explored one can occur in densified glasses displaying anomalous behavior on the elastic moduli, hereinafter referred to as elastic modulus anomaly (EMA). The EMA was recognized in vitreous silica either after cold- or hot-compression, observed in the initial densification region [8, 9]. As the usual nomenclatures in glass science, cold-compression refers to the compression performed at room temperature, whereas the hot-compression is performed at higher temperatures, yet below the glass transition temperature (Tg).Deschamps *et al.* [8] performed an ex-situ Brillouin investigation of cold-densified vitreous silica, submitted to different maximum pressures, and reported an anomalous behavior for the longitudinal sound velocities as a function of the densification ratio. After cold-compression, vitreous silica exhibits EMA for glasses densified between 9 and 12 GPa. These pressures correspond to the elastic limit and a 5% densification ratio [10]. Hot-compression of vitreous silica presenting a 2% densification ratio compared to pristine glass also yields EMA [11], which is completely vanished at a 9% densification ratio. The lack of intermediate data between these densification ratios, obtained after compression at 500 ^{o}C and 4 GPa or 6 GPa [11], precludes a more detailed EMA description midway.

In both pressure-induced anomalous behaviors, namely EA and EMA, the longitudinal sound velocity decreases with small density variations, recovering its normal increasing behavior when the density increment is more significant. Regarding their distinctions, EA occurs during compression in the elastic regime probed in-situ, whereas EMA is observed in densified glass, *i.e.* after a plastic compression-decompression cycle. In densified vitreous silica, the EMA presents a

less pronounced minimum in sound velocity and invariant elastic moduli up to a 5% densification ratio [12].

Given that silica is the archetypal glass, and the system $PbO\text{-}SiO_2$ can form glass over a wide range of compositions, unraveling the nuances of its structure - either pristine or under pressure - may offer a verdict of the debatable role of Pb in these glasses and even guide the choice of ecological substitutes offering similar properties. The pressure effect on the mechanical properties of these glasses has been investigated by Yoshimoto and co-workers [13, 14]. In the first contribution, they conducted in-situ acoustic resonance investigations for glass compositions ranging from 0 to 70 mol.% PbO. By the elastic moduli variations up to 100 MPa, they verified that with increasing PbO content the EA decreases, leading to a normal behavior above 30 mol.% PbO [13]. The same group has also studied the effect of the hot-densification on the elastic moduli of $PbO\text{-}SiO_2$ glasses after compression at 6 GPa and 0.75*Tg. The resulting pressure treatment at these fixed conditions showed densification rates decreasing monotonically with lead content, while hardness and Young's modulus display a minimum at 50 mol.% PbO (PS). Although these studies provide a general pressure behavior as a function of the lead content, with mechanical enhancements more modest to the PS than any composition in the glass system, the variable pressure is underexplored.

Brillouin spectroscopy is a powerful inelastic scattering method that probes the matter as a continuum, ultimately enabling the determination of the propagation velocities of elastic waves, and therefore their elastic characterization, even at extreme conditions [15]. In this paper, we investigated with such a spectroscopy the refractive index weighted sound velocity of PS glass as a function of pressure, and maximum pressure reached in irreversible pressure cycles. A series of samples underwent different maximum pressures in a diamond anvil cell (DAC) and a macroscopic sample submitted to 5 GPa in a Belt press apparatus. The combination of Brillouin and ellipsometric probes furnishes the longitudinal sound velocity and refractive index for the macroscopically densified and uncompressed glasses providing evidence to EMA. We also investigated cold-compression in-situ by Brillouin and Raman probes in order to understand the pathways resulting in this atypical phenomenon driven by densification.

2. Experimental Procedures

2.1. Samples Preparation

$PbSiO_3$ (PS) glass samples from two distinct batches were investigated. These glass batches were produced by the usual melt-quenching method from ground quartz SiO_2 (Vitrovita, Brazil) and Pb_3O_4 (Sigma-Aldrich, USA), further annealed close to the glass transition temperature (Tg = 687 K [16, 17]) and slowly cooled in order to relieve residual stresses in the pristine glasses [18].

Chemical compositions from the batches were verified by electron probe microanalysis (EPMA) on a JEOL JXA8230 5-WDS using a 15 nA current and 15 kV voltage on a 1 μm spot size in different points, exhibiting homogeneous composition. The average compositions of the glass batches (Table 1) are accurate to the nominal lead to silica proportion within an estimated uncertainty of ± 0.5 mol.%.

Table 1: Chemical compositions of the PS glass batches.

	PbO (mol.%)	**SiO_2 (mol.%)**
DAC samples	50.3	49.7
Belt Press samples	50.1	49.8

The microscopic PS specimens compressed in the diamond anvil cell (DAC) are from the same batch as in these works [16, 18-21], compressed as-prepared. The macroscopic PS sample submitted to high-pressure in the Belt press is from a distinct batch, cut to guarantee geometric requirements, i.e. face parallel cylinder displaying $5.7 \pm 0.1\ mm$ in height and $3.95 \pm 0.05\ mm$ in diameter. Spectroscopic ellipsometry measurements required mechanical polishing on one side to increase the signal-to-noise ratio, and reduce depolarization effects arising from non-uniform surface scattering. The cold-compressed and uncompressed glass samples underwent optical polishing and subsequent cleaning with acetone, which were performed equivalently to both samples.

2.2. High-Pressure Processing

PS samples were cold-compressed in a Chervin-type DAC. The typical sample size is 50 × 50 × 20 μm^3, placed within a 200 μm diameter and 50 μm height chamber in a stainless-steel gasket. A 4:1 methanol-ethanol mixture was used as the transmitting medium, remaining hydrostatic up to 10.5 GPa and quasi-hydrostatic above [22]. The pressure calibration was deduced from the shift of the R1 fluorescence Cr^{3+} line ($^2E \rightarrow {}^4A_2$) of ruby chips excited with a 532 nm laser

[23]. Pressure within the DAC apparatus was determined using multiple ruby chips before and after each vibrational spectrum acquisition, to ensure its accuracy and estimate uncertainties. We performed two in-situ pressure runs under comparable pressure conditions, enabling independent acquisition by Raman and Brillouin probes. The spatial and temporal pressure averages in these runs were evaluated as labeled. The pressure errors were estimated to be ±0.1 GPa within the hydrostatic pressure region; ±0.5 GPa until 16 GPa; and ±1 GPa above 16 GPa.

A macroscopic PS sample was cold-densified in a high-pressure Belt type press at 5 GPa, settled at the apparatus pressure limit. The sample cylinder was enclosed by a boron nitride crucible and introduced inside a carbon tube. The assembly was inserted in a pyrophyllite gasket, which served as a transmitting medium. The pressure was incremented (5 bar/min) up to 5 GPa, where the entire system was kept for 10 minutes, followed by a smooth decompression (1 bar/min) that took about four hours. At the end of the process, we recovered a fragmented sample composed of discs and smaller pieces.

2.3. Analytical Techniques

In-situ Raman measurements were taken along a complete pressure cycle up to 22±1 GPa, using a LabRAM HR micro-Raman spectrometer from Horiba Jobin Yvon with a 532 nm laser wavelength excitation source. Although its high hydrostatic limit, the applied alcohol solution presents Raman modes centered at room condition on 882 and 1032 cm^{-1} [24], assigned to the stretching modes of C-C in methanol and C-O in ethanol, respectively. These parasitic bands precluded an in-situ characterization of the high-frequency region of PS glass, attributed to Si-O stretching modes [21].

Brillouin scattering measurements were recorded using a Sandercock tandem Fabry Perot coupled with a microscope in back-scattering geometry. A λ_0=532 nm green Nd^{3+}:YAG laser source was used to excite the samples. Long accumulation time was necessary to get a good signal-to-noise ratio in spectra, which in some cases were acquired overnight. The reported peak positions correspond to the average of the Stokes and anti-Stokes absolute values to the Brillouin frequency, estimated by curve-fit the peaks with Lorentzian functions. In-situ Brillouin data were conducted for a unique specimen from ambient pressure up to 20±1 GPa, on the compression and decompression paths. Ex-situ Brillouin measurements were performed considering the set of densified PS glasses investigated here [21] and the Belt press samples.

Density and ellipsometric measurements were conducted to the macroscopic Belt press samples cold-compressed at 5 GPa and uncompressed. Densities were estimated at room condition through the buoyancy method based on Archimedes's principle using distilled water as the immersion liquid. Spectroscopic ellipsometry measurements were obtained using a J.A. Woollam Co. rotating compensator ellipsometer M-2000 in a wide wavelength range, from 193 nm to 1000 nm, probing 500 points. Such measurements require a millimeter sample size, with the limitation given by the incident light beam diameter. In order to maximize the sensitivity, ellipsometric angles (Ψ,Δ) were acquired close to the Brewster angle at 55°, 60° and 65°. The (Ψ,Δ) data of the single reflection measured from the bulk material were mathematically inverted to obtain the optical constants of the samples. To confirm results, Kramer–Kronig consistent models based on Lorentz oscillators, were used to reproduce the presence of absorption in the UV region and to determine the optical properties in the whole measurement region.

3. Results

3.1. In-situ High-Pressure Raman Scattering

The in-situ Raman spectra as a function of the pressure upon compression (Fig.1a) and decompression (Fig.1b) present spectral modifications in the low-frequency region (< 200 cm^{-1}). This region comprises three peaks: the Boson peak (40 cm^{-1}), which is observed in glass matter [25]; and two peaks centered at 95 cm^{-1} and 135 cm^{-1} at room pressure, both assigned to Pb-O vibration, as present in other lead-bearing glass systems [26-29]. At high pressures, Raman spectra display an inversion relationship to the intensity of the low-frequency peaks: decreasing the Boson peak intensity [30-32] and favoring the peak centered at 95 cm^{-1}, gradually suppressing the 135 cm^{-1} peak. These changes are partially recovered back at room condition, as suggests the spectral profile that returns about the same features, except for the small redshift of the peak initially located at 135 cm^{-1} (Fig.1c).

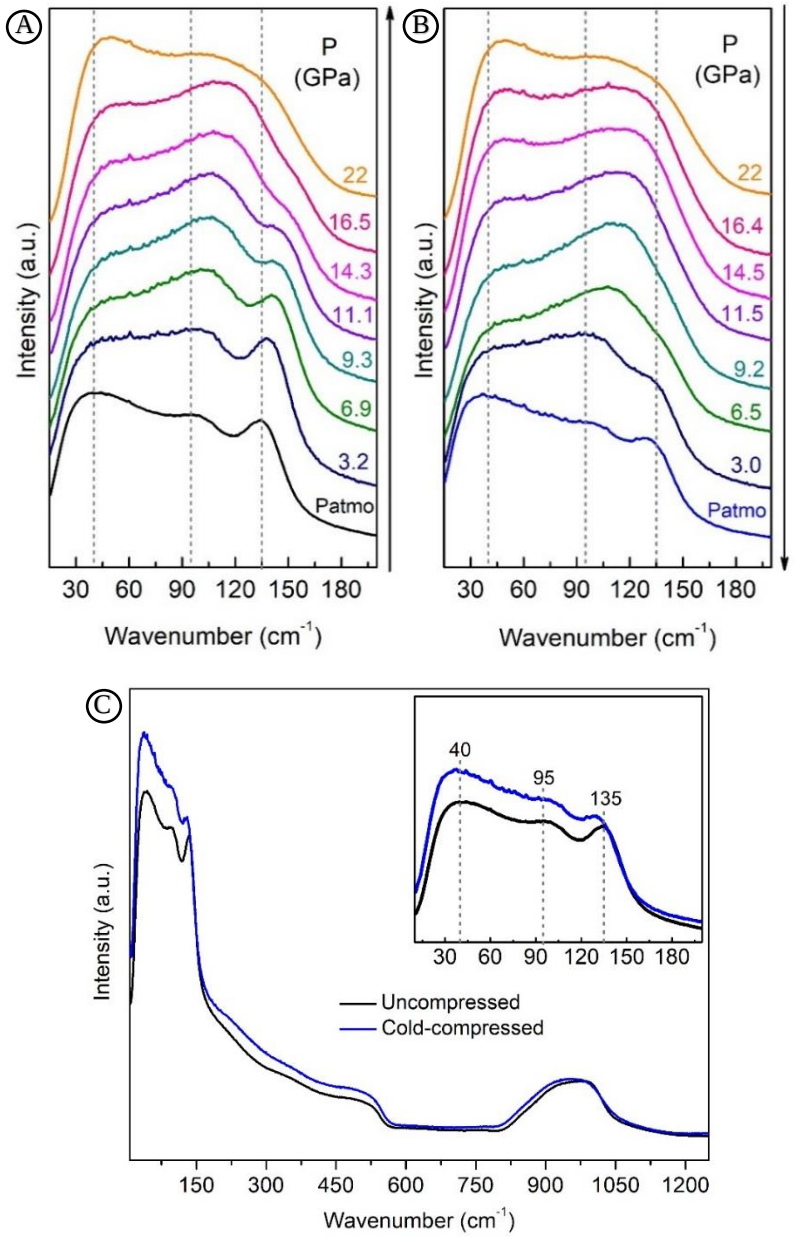

Figure 1: The effect of the pressure in this spectral region was recorded in-situ in a complete (a) compression and (b) decompression cycle in the DAC. (c) Raman spectra recorded ex-situ for cold-compressed at 22 GPa and uncompressed PS samples. The inset details the low-frequency region displaying the Boson peak and two peaks attributed to Pb-O vibrations, with the dashed lines marking the initial center positions for these peaks.

3.2. In-situ High-Pressure Brillouin Scattering

Figure 2 presents the in-situ Brillouin shift (v_L) as a function of pressure for PS glass for a complete compression and decompression cycle. The entire compression path is well adjusted by a linear function, while the decompression requires a polynomial function of at least the second degree for a good fit.

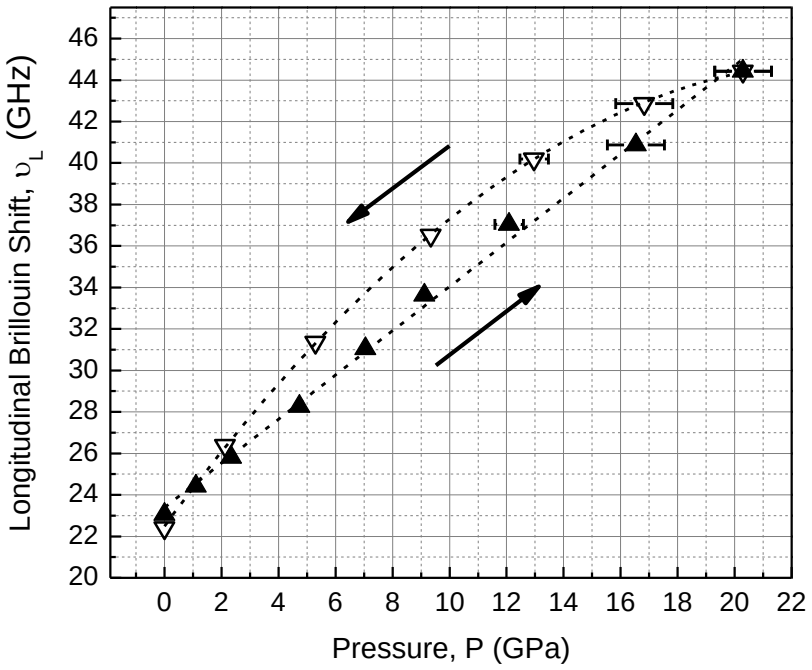

Figure 2: In-situ longitudinal Brillouin line shift (v_L) of PS glass up to 20 GPa in a complete compression and decompression cycle in the DAC.

The pressure range from 2 GPa to 20 GPa shows slightly higher v_L values during decompression. Nevertheless, at the end of the compression-decompression cycle, the effect of densification on PS glass results in a slightly lower Brillouin frequency than the initial pristine glass, $v_L = 22.4$ GHz and 23.4 GHz, respectively. In the next section, we discuss this atypical observation by analyzing ex-situ PS glass samples released from different maximum pressures (P_{max}).

3.3. Ex-situ High-Pressure Brillouin Scattering

Figure 3 displays the change in longitudinal Brillouin shift v_L values (Fig.3a) along with their respective spectra (Fig.3b) for the set of densified PS samples submitted to different P_{max} in DAC, same samples of reference [21]. Such new reinvestigation performed here is three-fold: (i) It provides a complementary description of the pressure-induced modifications in different scales. High-frequency Raman scattering indicated slight changes in the glass depolymerization, corresponding to the short-range ordering scale whereas Brillouin spectroscopy probes the matter as a continuum medium. (ii) As a straight consequence, it addresses the elastic properties allowing an alternative estimation of the elastic and plastic saturation limits. (iii) Last but not least, it sheds

light on the atypical decrease in Brillouin frequency observed in the PS specimen densified at 20 GPa.

Firstly, we corroborate for cold-densified PS samples the elastic and plastic saturation limits evaluated with the barycenter of the high-frequency region of the Raman spectra, from 790 cm^{-1} to 1200 cm^{-1} [21]. This previous study estimated the elastic limit around 4 GPa, as above plastic deformations occur with progressive network depolymerization. These irreversible modifications cease for densified glass that underwent P_{max} above 20 GPa.

The longitudinal Brillouin shift decreases monotonically with P_{max} (Fig.3a); following the same tendency as shown in Figure 2 for the glass retrieved after a compression-decompression cycle to 20 GPa. The measured frequency v_L is proportional to the product of the refractive index (n) and the longitudinal sound velocity (v_L):

$$v_L = \frac{2n \cdot v_L}{\lambda_0} \qquad (1)$$

where λ_0 is the laser excitation wavelength.

The decrease of v_L as a function of P_{max} reveals a diminution in the magnitude of at least one of these parameters, either n or v_L, for the full set of densified PS glass above the elastic limit.

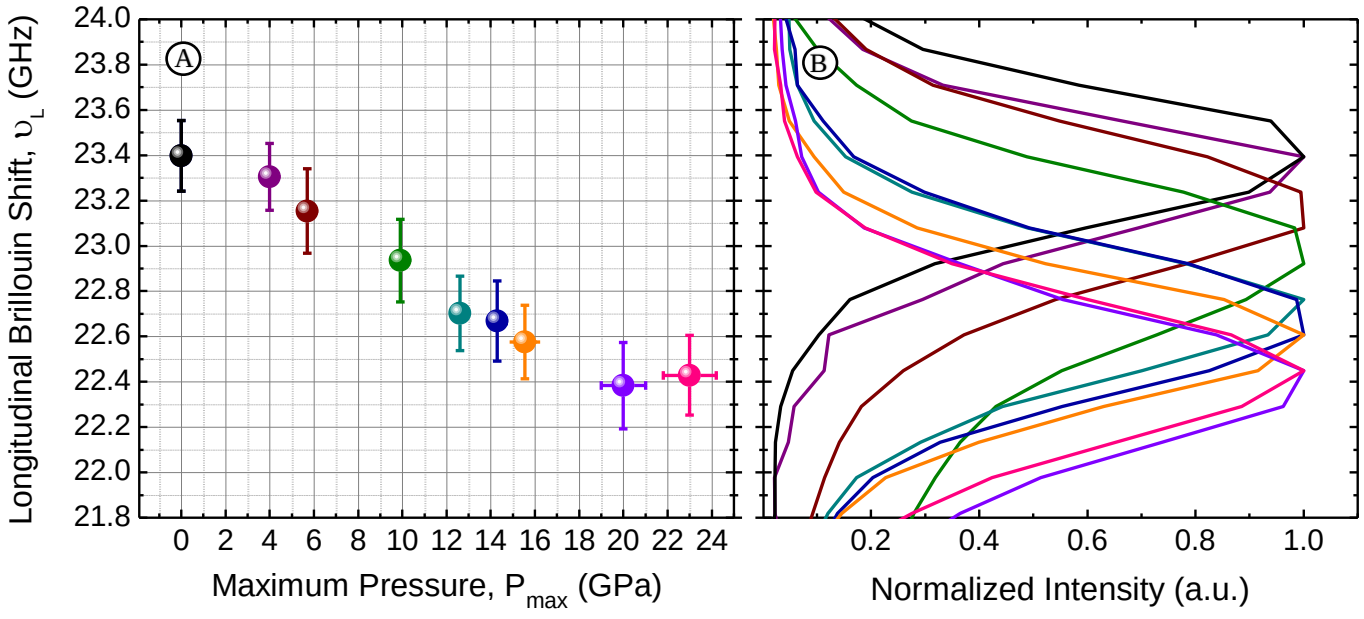

Figure 3: (a) Longitudinal Brillouin line shift (v_L) as a function of the maximum pressure (P_{max}) and (b) Brillouin spectra of the uncompressed and cold densified PS samples. Brillouin measurements were recorded at atmospheric pressure after a complete compression-decompression cycle in the DAC apparatus. Uncertainties in the Brillouin values were evaluated as one-eighth of the related line width.

3.4. Ex-situ Refractive Index and Elastic Moduli Variation

Due to the low elastic limit confirmed by Brillouin spectroscopy at ~ 4 GPa, cold-compression at the maximum pressure attained in the Belt apparatus (5 GPa) is irreversible and then enables to obtain a macroscopic 'densified' sample. From spectroscopic ellipsometry, the behavior of the real part (n) and extinction coefficient (κ) of the refractive index reveals sensible pressure-induced modifications (Figure 4).

In agreement with the classical electromagnetic theory, we observe higher n values for the densified in respect to the uncompressed glass in the full wavelength range probed. For Brillouin comparison purposes (λ_0=532 nm), n is estimated as 1.878± 0.008 and 1.843± 0.008, respectively. Then, for the 5 GPa cold-densified glass, the refractive index increases by 1.9% compared to pristine glass.

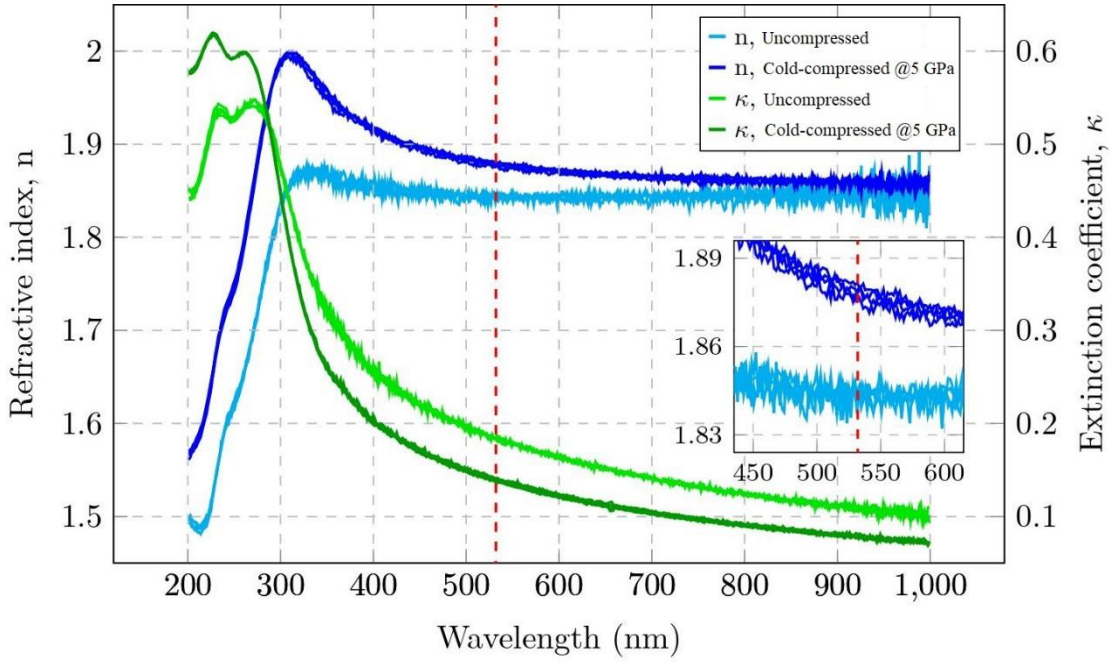

Figure 4: Real part (n) and extinction coefficient (κ) of the refractive index, obtained at 55°, 60°, and 65°, for the Belt cold-compressed at 5 GPa and uncompressed PS samples obtained upon direct inversion. The dashed line at λ=532 nm marks the Brillouin probing wavelength with the respective n values zoomed in the inset.

Measurements using Archimedes's principle show within the error bar no modification between the density of the macroscopic cold-compressed and the uncompressed glasses ($\rho = 5.85 \pm 0.02\ g.cm^{-3}$). From the literature, PS glass hot-compressed at 6 GPa and ~230 °C shows a 2.6% densification [14]. Even if we apply here comparable pressures, it is long known that hot-

compression yields larger densification rates [33]. Historically, pressure-treated glasses above the elastic limit are referred to as 'densified', being interchangeable nomenclatures. Strictly, densification implies an irreversible increase in the glass density. We highlight the potential of spectroscopic means in determining the elastic limit either by exploring pressure-sensitive properties ($n, \mathrm{v}_L, n{\cdot}\mathrm{v}_L$) and/or by short-range structural description (coordination, polymerization).

The combination of longitudinal Brillouin, ellipsometric, and buoyancy measurements performed in macroscopically densified specimens indicates a slightly lower longitudinal elastic modulus after cold-compression at 5 GPa (Table 2). The pristine values for n, v_L, ρ and L are close to the ones reported in the literature [13, 34-36].

Table 2: Longitudinal Brillouin shifts (ν_L), refractive indices (n), longitudinal sound velocities (v_L), densities (ρ), and longitudinal elastic moduli (L) for pristine and cold densified glasses from Belt press.

	ν_L (GHz)	n	v_L ($m.s^{-1}$)	ρ ($g.cm^{-3}$)	L (GPa)
Uncompressed	23.54±0.09	1.843±0.008	3398±20	5.85±0.02	67.5±0.8
Cold-densified at 5 GPa	23.39±0.08	1.878±0.008	3313±20	5.85±0.02	64.2±0.8

4. Discussion

4.1 In-situ High-Pressure

Upon compression, the positive slope coefficient of the Brillouin shift as a function of pressure ($\frac{\partial\, \nu_L}{\partial \mathrm{P}} = 1.0\ \mathrm{GHz.\,GPa^{-1}}$) evidences that PS glass displays a normal behavior and does not present the EA, as observed in silica glass. During decompression, the curvature of ν_L is also closer to that of depolymerized silicates than to vitreous silica [4, 37].

The absence of the EA in PS glass agrees with Yoshimoto *et al.*[13], who studied the PbO-SiO_2 system, reporting normal increasing behavior for compressed lead silicate glasses with PbO content greater than 30 mol.%, but for maximum pressure up to 100 MPa. Similar behavior was reported in sodium aluminosilicate glasses with varying initial depolymerization degrees [4]. Structurally, vitreous silica is a fully polymerized glass composed of SiO_2 tetrahedra forming a 3D network constituting of different sized rings, where 6-membered rings dominate [38]. The EA observed in silica and silicate glasses under pressure is attributed to a polyamorphic $\beta \rightarrow \alpha$ cristobalite-like transition occurring on 6-membered silicate rings. This transition has been interpreted by an abrupt angular rotation of the Si-O-Si bond without bond breaking or creation, featuring modifications on the ring conformation, followed by a narrowing in the inter-tetrahedral

angle distribution, as evidenced by molecular dynamic simulations [39] and Raman scattering measurements [12, 40].

In the PbO-SiO_2 glass system, lead incorporation induces progressive silica network depolymerization, through the breakdown of Si-O-Si linkages, forming non-bridging oxygens (NBO). This process contributes to the destruction, either partial or complete, of the silica ring structure [4]. Indeed, molecular dynamics (MD) simulations showed that the intermediate-range order in PS lacks the 3D connectivity within the network and the dominant presence of 6-membered rings [41-43].

In silicate glasses, the Q^n population (with n ranging from 0 to 4) describes the glass structure in terms of network polymerization. At ambient conditions, PS glass presents well-defined tetrahedral silicon sites organized mostly as Q^2 entities interconnected with the other two silicon tetrahedra [16, 44-47]. Our recent Raman investigation shows that the PS glass densification prompted a slight conversion of more polymerized (Q^3 and Q^4) to less polymerized (Q^1 and Q^0) tetrahedra, increasing the proportion of NBO. Focusing on the ordering around lead, despite the lack of consensus in the literature about the structural role played by these cations as a function of the glass composition, structural studies performed in the last two decades converge to PbO_3 and PbO_4 pyramids ($n = 3, 4$) [41, 47-51], excluding the ionic octahedral coordination suggested in primary XRD investigations [52-55].

To the best of our knowledge, there are no previous in-situ spectroscopic investigations of lead silicate glass under pressure to aid in building a structural description. High-density MD simulations conducted on lead silicate glass and melts indicate the presence of highly coordinated Pb and Si polyhedra [42, 43, 56, 57]. These studies for the melt also appoint to lack of deformation to silicon polyhedra, as the Si-O bond lengths and angles are almost unaffected [56, 57], whereas the local arrangement around Pb is strongly pressure-dependent [57]. In other words, these simulations indicate that Pb polyhedra are likely more deformable than Si polyhedra in response to high-pressure.

Hagiwara *et al.* [58] first attributed the Raman peak at 135 cm^{-1} to the vibration of the Pb^{2+} ion. Afterward, it was recognized as being analogous to those peaks found on isochemical crystalline phases [59-61] and lead oxides [61], indicating the existence of Pb-O covalent bonding. Zahra et al. [62] ascribed both of the low-frequency Pb-O peaks to the PbO_4 pyramids, specifying the peak at 135 cm^{-1} as due to symmetric stretching vibrations of these polyhedra. Such assignment

agrees with partial reports conducted on these glasses [59, 63, 64]. Because of the PbO_4 attribution, our observed modifications to the Pb-O peaks suggest a progressive change in the Pb environment possibly extending from minor deformation within the tetragonal pyramids (*e.g.* Pb-O bond lengths and internal angles) to the formation of highly coordinated PbO_n polyhedra.

Continuous modifications of Pb coordination correlate well with the in-situ linear variation to $n \cdot v_L$ upon compression. As a comparison with other silicates, in-situ Brillouin investigation of anorthite ($CaAl_2Si_2O_8$) glass reported the Al coordination to change continuously upon compression, whereas the abrupt modification of $n \cdot v_L$ at 5 GPa is attributed to the formation of fivefold coordinated silicon [3]. In enstatite ($MgSiO_3$) glass, in-situ Brillouin probes revealed a change in the slope of v_L at 8 GPa and 18 GPa, associated with polyamorphic phase transitions, ascribed to pressure dependence of the Si-O-Si angle and formation of highly coordinated silicon, respectively [37]. In the case of PS glass, changes in Si coordination and polyhedral connectivity at high pressure are open issues that could aid to describe the structural modifications and densification mechanisms.

4.2. Ex-situ High-Pressure

After an irreversible compression-decompression cycle, the $n \cdot v_L$ product is usually reported to increase [3, 4, 8, 65]. An exception to this rule is enstatite, which displays within the experimental error identical v_L to the densified and uncompressed glass [37]. Another more puzzling exception is the PS glass, which exhibits a monotonic decrease in $n \cdot v_L$ with P_{max} for the full pressure range above the elastic limit. Spectroscopic ellipsometry measurements of our Belt press samples reveal refractive indices increasing with the densification ratio at 5 GPa, which appoints to an even more remarkable decrease in the magnitude of v_L.

Regarding cold-densified vitreous silica, the refractive index increases monotonically, while v_L displays a minimum for a densification rate of 5%, decreasing for maximum pressures within the 9 to 12 GPa range [8]. In this case, the positive increment in n masks the v_L slowdown since $n \cdot v_L$ increases gradually with the maximum pressure reached. An initial decrease in v_L was also observed in hot-densified vitreous silica [11]. In this case, the longitudinal Brillouin frequency also decreases with the densification ratio, due to a less prominent increase in n.

Vitreous silica is a classical exception to the normal variation of the elastic moduli upon compression, exhibiting jointly EA and EMA anomalous behaviors. Deschamps *et al.* [8]

attributed the diminution in the sound velocities at the beginning of the permanent densification to gradual polyamorphic $\beta \rightarrow \alpha$ cristobalite-like transition, analogous to the elastic structural mechanisms that explain the EA. This same structural mechanism is unlikely to explain our data, at least not strictly, as the PS glass does not present the classical EA due to its depolymerized silicate network, reported to be slightly enhanced with densification [21]. It is remarkable, from the PS glass behavior that EMA can occur independently from EA.

Huang *et al.* [66] explained the anomalous elastic behavior in vitreous silica by the polyamorphic $\beta \rightarrow \alpha$ cristobalite-like transition through the glass ability to undergo irreversible densification. According to these authors, the decreasing of the void space plays an important role in reducing locally the glass capability to undergo structural ring conformation transition. In this regard, EMA observed in vitreous silica links straightly to the small variations of density, by up to 5% in cold-compressed and 2% in hot-compressed glass, both in the beginning densification ratios, which can reach up to 21%. Due to the lack of information in the literature approaching the PS maximum densification capability, we estimate this value through Rouxel`s model [67] based on Poisson`s ratio (σ) of pristine PS glass, the same procedure was also adopted there [68] . For σ = 0.259 [13], Rouxel`s empirical model predicts a 5.2% maximum densification driven by compression [67]. In this model, at a comparable Poisson`s ratio as the PS composition, the window glass deviates negatively from the empirical curve, which could be associated with a densification capability even lower than the aforementioned estimated for PS. As a matter of comparison, the only densification ratio reported scales to 2.6%, as obtained by Yoshimoto after hot-compression, which does not claim to be maximal.

For the macroscopic PS sample densified in the Belt press, sensible density modification is not observed whereas v_L decreases, resulting in elastic longitudinal modulus drop driven by cold-compression (Table 2). The cold-compression to different P_{max} in the DAC led to negative variations in $n \cdot v_L$, scaling $\Delta v_L = -4.5\%$ for the sample densified at 20 GPa. The elastic moduli for the microscopic densified PS glass above 5 GPa require the values of v_L and ρ at the same conditions. However, if the same trend observed in the macroscopic sample also occurs in the microscopic ones, that is, decreasing in the longitudinal sound velocity $\left(\text{i. e., } \frac{dv_L}{dP_{max}} < 0\right)$. Since the longitudinal modulus (L) is:

$$L = \rho v_L^2 \qquad (2)$$

Hence, the pressure derivative of L is given by:

$$\frac{dL}{dP_{max}} = \frac{d\rho}{dP_{max}} \mathrm{v}_L^2 + 2\rho \mathrm{v}_L \frac{d\mathrm{v}_L}{dP_{max}}, \quad (3)$$

being the second term negative.

In the situation where the densification is marginal, the negative term becomes more relevant, resulting in a decreasing longitudinal elastic modulus driven by pressure. This way, we suggest that, in densified glass, EMA can be associated with a marginal density increase whereas v_L decreases with P_{max}. Hence, cold-densified PS glass is a presumable candidate to exhibit EMA in the full pressure range above the elastic limit.

On the other hand, the hot-compressed PS glass investigated by Yoshimoto *et al.* [14] displays a 2.6% densification accompanied by an increase in the hardness and Young`s modulus (v_L by inference) values, indicating the influence of structural factors affecting the v_L behavior. These opposite changes to v_L are possibly related to the distinct pressure treatments applied. As a result of hot-compression, Svenson *et al.* [69] observed an overall increase in elastic moduli across different compositions, correlated with density increment despite intrinsic structural distinctions among the glasses. These authors associate the increase in density with the atomic packing factor. Zeidler *et al.* [70] propose the oxygen-packing fraction, which scales with eventual coordination modification, to induce structural transformations driven at extreme P,T conditions. Indeed, some studies [71, 72] evaluating the glass atomic packing density across different glass families report its positive correlation with the Poisson ratio, highlighting the unambiguous influence of the structural configuration on the elastic properties.

Glass properties are functions of composition, temperature, and pressure, but also from their thermal and pressure histories. Departing from the same pristine glass composition, different pressure and temperature routes can yield the same densification rates, although such varying treatments may give rise to glass with intrinsically distinct structures, as put in evidence studies conducted in vitreous silica [9, 73]. Martinet *et al.* [73] reported an increase in 3-membered rings as a function of density in cold compressed vitreous silica, whereas they did not observe different hot-compression isotherms affecting the statistics of 3-membered rings. From their X-ray diffraction and vibrational experiments, Guerette *et al.* [9] also provided evidence of different intermediate-range orders arising from distinct compression routes, ascribing the Raman modifications observed by Martinet *et al.* [73] to rearrangements in the network structure to which

3-membered rings are bonded. Noteworthy, even exhibiting distinct features to the intermediate-range structure, EMA is observed in vitreous silica densified through either cold or hot compression, at the beginning of the densification range.

It is tempting to associate the decrease in the longitudinal sound velocity in PS glass with structural modification in the short-range ordering. In a recent elastic study performed in the SiO_2-TiO_2 glass system, Williams *et al.* [74] highlighted that the coordination transition is not easily detectable in the bulk and shear modulus, since other structural changes might concurrently take place in these glass structures, such as weaker polyhedral bonds. Grammes *et al.* [68] draw a similar manyfold conclusion in multicomponent aluminosilicate glass, appointing network polymerization and atomic packing density as factors contributing to elastic moduli modification. As regards the correlation between anionic structure and elastic properties, shear and Young's moduli are reported to decrease with the increase of NBO in ternary sodium magnesium silicates [75]. In the case of cold-densified PS glass, depolymerization seems to play an important role in the final elastic properties, whereas it is still uncertain to detail the cation coordination modification driven by pressure.

In the PbO-SiO_2 system, higher PbO content gives rise to glasses with higher densities [35]. With increasing PbO content, the refractive indices are reported to increase [36, 76] whereas the longitudinal and transverse sound velocities decrease [13, 76]. These observations suggest that cold-compression acts on this glass somewhat similarly to a lead composition increment: increasing refractive index and decreasing the sound velocities, whereas density increases marginally. We aim to explore in a future contribution the structural distinctions through cold- and hot-compression in these glasses, given that hardness and elastic moduli increase by the last treatment [14, 69]. In this regard, mechanical properties resulting from pressure treatment may distinguish from a simple lead increment, resulting in a tailored combination of properties. A comprehensive description of the pressure effect on the mechanical properties can aid to design lead silicates glass for prospective commercial applications, such as radiation shielding [34, 77].

Conclusions

High-pressure elastic investigations of lead metasilicate (PS) glass were conducted by vibrational spectroscopies. Brillouin investigation of cold-densified PS glass corroborates the elastic and saturation limits estimated previously by Raman spectroscopy from the spectral high-frequency region.

In-situ Brillouin probes confirm the lack of the elastic anomaly (EA), while in-situ Raman probes present modifications in the spectral low-frequency region suggesting a continuous modification of the lead coordination at high pressures. A short-range structural description is necessary in order to understand the densification mechanisms in these glasses.

Ex-situ Brillouin probes unveil an abnormal decrease in the product between the refractive index and longitudinal sound velocities for the full set of cold-densified PS glass. Spectroscopic ellipsometry measurements of a macroscopic sample cold-densified at 5 GPa show that the refractive index increases whereas the longitudinal sound velocity decreases. Such slowdown in longitudinal sound velocity, accompanied by minor density increase, results in elastic modulus anomaly (EMA), leading to smaller longitudinal modulus after densification.

Acknowledgments

We are extremely thankful to José Rodrigues da Silva (LaMaV, UFSCar) and Philippe Veber (ILM, UCB Lyon 1) for their invaluable aid in producing and conforming the Belt press sample. The authors are grateful to São Paulo Research Foundation (FAPESP) for funding this research through the CEPID project no. 2013/07793-6, the Brazilian grant no. 2017/11868-2 and Brazil-France cooperation grant no. 2019/11446-6. We are also thankful to CNRS-UCB Lyon 1 for their financial support. EDX measurements were performed at the Geology Department, at the University of Toronto. The high-pressure experiment conducted in a Belt press apparatus was performed at the Lyon Platform of Experiments under Extreme Conditions (ILMTech-PLECE). Brillouin and Raman experiments were carried out at the vibrational spectroscopies Platform at University Lyon 1- France (ILMTech-CECOMO).

References

1. Bridgman, P.W., *The thermal conductivity and compressibility of several rocks under high pressures.* American Journal of Science, 1924. **s5-7**(38): p. 81.
2. Bridgman, P.W., *Compressibility of glasses.* American Journal of Science, 1925. **s5-10**(58): p. 359.
3. Moulton, B.J.A., et al., *Structure—longitudinal sound velocity relationships in glassy anorthite ($CaAl_2Si_2O_8$) up to 20 GPa: An in situ Raman and Brillouin spectroscopy study.* Geochimica et Cosmochimica Acta, 2019. **261**: p. 132-144.
4. Sonneville, C., et al., *In situ Brillouin study of sodium alumino silicate glasses under pressure.* The Journal of Chemical Physics, 2013. **139**(7): p. 074501.
5. Kondo, K.i., S. Iio, and A. Sawaoka, *Nonlinear pressure dependence of the elastic moduli of fused quartz up to 3 GPa.* Journal of Applied Physics, 1981. **52**(4): p. 2826-2831.
6. Polian, A. and M. Grimsditch, *Sound velocities and refractive index of densified a-SiO_2 to 25 GPa.* Physical Review B, 1993. **47**(21): p. 13979-13982.
7. Zha, C.-s., et al., *Acoustic velocities and refractive index of SiO_2 glass to 57.5 GPa by Brillouin scattering.* Physical Review B, 1994. **50**(18): p. 13105-13112.
8. Deschamps, T., et al., *Elastic Moduli of Permanently Densified Silica Glasses.* Scientific Reports, 2014. **4**(1): p. 7193.
9. Guerette, M., et al., *Structure and Properties of Silica Glass Densified in Cold Compression and Hot Compression.* Scientific Reports, 2015. **5**: p. 15343.
10. Deschamps, T., et al., *Permanent densification of compressed silica glass: a Raman-density calibration curve.* Journal of Physics: Condensed Matter, 2012. **25**(2): p. 025402.
11. Zanatta, M., et al., *Elastic properties of permanently densified silica: A Raman, Brillouin light, and x-ray scattering study.* Physical Review B, 2010. **81**(21): p. 212201.
12. Deschamps, T., et al., *Elastic anomalous behavior of silica glass under high-pressure: In-situ Raman study.* Journal of Non-Crystalline Solids, 2009. **355**(18): p. 1095-1098.
13. Yoshimoto, M. and N. Soga, *Elastic Properties and the Short- and Medium-Range Structures of Lead Silicate Glasses.* Yogyo-Kyokai-Shi(J. Ceram. Soc. Jpn.), 1986. **94**(10): p. 1041-1048.
14. Yoshimoto, M., et al., *Effects of densification on mechanical properties of lead silicate glasses.* Journal of the Ceramic Society of Japan, 1989. **97**(1132): p. 1446-1450.
15. Vincent, B., et al., *Spectroscopie Brillouin : introduction et exemples*. 2020. p. 247-272.
16. Sampaio, D.V., et al., *Raman scattering and molecular dynamics investigation of lead metasilicate glass and supercooled liquid structures.* Journal of Non-Crystalline Solids, 2018. **499**: p. 300-308.
17. Silva, D.C., et al., *Synthesis of $PbO{\cdot}SiO_2$ glass by CO_2 laser melting method.* Journal of Non-Crystalline Solids, 2019. **522**: p. 119572.
18. Felipe Lancelotti, R., et al., *Is the structural relaxation of glasses controlled by equilibrium shear viscosity?* Journal of the American Ceramic Society, 2021. **104**: p. 2066-2076.
19. Pena, R.B., et al., *In-situ Raman spectroscopy unveils metastable crystallization in lead metasilicate glass.* Journal of Non-Crystalline Solids, 2020. **546**: p. 120254.
20. Cassar, D.R., et al., *Elemental and cooperative diffusion in a liquid, supercooled liquid and glass resolved.* The Journal of Chemical Physics, 2017. **147**(1): p. 014501.
21. Pena, R.B., et al., *High-pressure plastic deformation of lead metasilicate glass accessed by Raman spectroscopy: Insights into the Q^n distribution.* Journal of Non-Crystalline Solids, 2021. **567**: p. 120930.
22. Klotz, S., et al., *Hydrostatic limits of 11 pressure transmitting media.* Journal of Physics D: Applied Physics, 2009. **42**(7): p. 075413.
23. Mao, H.K., J. Xu, and P.M. Bell, *Calibration of the ruby pressure gauge to 800 kbar under quasi-hydrostatic conditions.* Journal of Geophysical Research: Solid Earth, 1986. **91**(B5): p. 4673-4676.

24. Lemos, V. and F. Camargo, *Effects of pressure on the Raman spectra of a 4:1 methanol–ethanol mixture.* Journal of Raman Spectroscopy, 1990. **21**(2): p. 123-126.
25. Malinovsky, V.K. and A.P. Sokolov, *The nature of boson peak in Raman scattering in glasses.* Solid State Communications, 1986. **57**(9): p. 757-761.
26. Morgan, S.H., D.O. Henderson, and R.H. Magruder, *Infrared and Raman spectra of lead fluorosilicate glasses.* Journal of Non-Crystalline Solids, 1991. **128**(2): p. 146-153.
27. Filho, A.G.S., et al., *Raman spectroscopy study of high B_2O_3 content lead fluoroborate glasses.* Journal of Raman Spectroscopy, 1999. **30**(7): p. 525-529.
28. Sigaev, V.N., et al., *Structure of lead germanate glasses by Raman spectroscopy.* Journal of Non-Crystalline Solids, 2001. **279**(2): p. 136-144.
29. Chakraborty, S., et al., *Anomalous variation of Boson peak and fragility and their correlations with intermediate-range structure in PbO-B_2O_3 glasses.* Journal of Alloys and Compounds, 2017. **713**: p. 95-107.
30. Schroeder, J., et al., *Raman scattering and Boson peaks in glasses: temperature and pressure effects.* Journal of Non-Crystalline Solids, 2004. **349**: p. 88-97.
31. Mantisi, B., et al., *Non-Debye normalization of the glass vibrational density of states in mildly densified silicate glasses.* Journal of Physics: Condensed Matter, 2009. **22**(2): p. 025402.
32. Deschamps, T., et al., *Silica under hydrostatic pressure: A non continuous medium behavior.* Journal of Non-Crystalline Solids, 2009. **355**(48): p. 2422-2424.
33. Mackenzie, J.D., *High-pressure Effects on Oxide Glasses: III, Densification in Nonrigid State.* Journal of the American Ceramic Society, 1964. **47**(2): p. 76-80.
34. Singh, K.J., et al., *Gamma-ray shielding and structural properties of PbO–SiO_2 glasses.* Nuclear Instruments and Methods in Physics Research Section B: Beam Interactions with Materials and Atoms, 2008. **266**(6): p. 944-948.
35. Ben Kacem, I., et al., *Structure and properties of lead silicate glasses and melts.* Chemical Geology, 2017. **461**: p. 104-114.
36. Dimitrov, V.V., et al., *Third Harmonic Generation in PbO-SiO_2 and PbO-B_2O_3 Glasses.* Journal of the Ceramic Society of Japan, 1993. **101**(1169): p. 59-63.
37. Sanchez-Valle, C. and J.D. Bass, *Elasticity and pressure-induced structural changes in vitreous $MgSiO_3$-enstatite to lower mantle pressures.* Earth and Planetary Science Letters, 2010. **295**(3): p. 523-530.
38. Rino, J.P., et al., *Structure of rings in vitreous SiO_2.* Physical Review B, 1993. **47**(6): p. 3053-3062.
39. Huang, L. and J. Kieffer, *Amorphous-amorphous transitions in silica glass. II. Irreversible transitions and densification limit.* Physical Review B, 2004. **69**(22): p. 224204.
40. Sonneville, C., et al., *Polyamorphic transitions in silica glass.* Journal of Non-Crystalline Solids, 2013. **382**: p. 133-136.
41. Rybicki, J., et al., *The structure of lead-silicate glasses: molecular dynamics and EXAFS studies.* Journal of Physics: Condensed Matter, 2001. **13**(43): p. 9781-9797.
42. Bergmański, G., et al., *The structure of rarefied and densified $PbSiO_3$ glass: a molecular dynamics study.* Task quarterly, 2004. **8**(3): p. 393-412.
43. Chomenko, K., et al., *The structure of porous and spontaneously densified amorphous $PbSiO_3$: A Molecular Dynamics Study.* Computational Methods in Science and Technology, 2004. **10**: p. 21-38.
44. Cormier, G., T. Peres, and J.A. Capobianco, *Molecular dynamics simulation of the structure of undoped and Yb^{3+}-doped lead silicate glass.* Journal of Non-Crystalline Solids, 1996. **195**(1): p. 125-137.
45. Schneider, J., et al., *Q^n distribution in stoichiometric silicate glasses: thermodynamic calculations and ^{29}Si high resolution NMR measurements.* Journal of Non-Crystalline Solids, 2003. **325**(1): p. 164-178.

46. Feller, S., et al., *A multispectroscopic structural study of lead silicate glasses over an extended range of compositions.* Journal of Non-Crystalline Solids, 2010. **356**(6): p. 304-313.
47. Fayon, F., et al., *^{29}Si and ^{207}Pb NMR study of local order in lead silicate glasses.* Journal of Non-Crystalline Solids, 1998. **232-234**: p. 403-408.
48. Fayon, F., et al., *Pb^{2+} environment in lead silicate glasses probed by Pb-L_{III} edge XAFS and ^{207}Pb NMR.* Journal of Non-Crystalline Solids, 1999. **243**(1): p. 39-44.
49. Takaishi, T., et al., *Structural Study on $PbO–SiO_2$ Glasses by X-Ray and Neutron Diffraction and 29Si MAS NMR Measurements.* Journal of the American Ceramic Society, 2005. **88**(6): p. 1591-1596.
50. Kohara, S., et al., *Lead silicate glasses: Binary network-former glasses with large amounts of free volume.* Physical Review B, 2010. **82**(13): p. 134209.
51. Alderman, O.L.G., et al., *Lead silicate glass structure: New insights from diffraction and modeling of probable lone pair locations.* Journal of the American Ceramic Society, 2022. **105**: p. 938– 957.
52. Bair, G.J., *The constitution of lead oxide-silica glasses: I, Atomic arrangement.* Journal of the American Ceramic Society, 1936. **19**(1-12): p. 339-347.
53. Krogh-Moe, J., *An X-Ray Investigation of Lead Silicate Glass1*, in *Zeitschrift für Physikalische Chemie*. 1958. p. 223.
54. Rabinovich, E.M., *Lead in glasses.* Journal of Materials Science, 1976. **11**(5): p. 925-948.
55. Takagi, Y., et al., *X-ray Diffraction Analysis of the $PbO–SiO_2$ System in the Glassy and the Molten State.* Transactions of the Japan institute of metals, 1985. **26**(7): p. 451-461.
56. Yen, N.V., et al., *Structural heterogeneity and dynamics in liquid $PbSiO_3$: insight from analysis and visualization of molecular dynamics data.* Materials Research Express, 2015. **2**(6): p. 065201.
57. Hong, N.V., et al., *Microstructure of lead silicate melt under compression: insight from computer simulation.* The European Physical Journal B, 2019. **92**(12): p. 268.
58. Hagiwara, H. and R. Oyamada, *Raman Spectra of Glassy $PbO-SiO_2$ System.* Journal of the Physical Society of Japan, 1974. **36**(3): p. 917-917.
59. Furukawa, T., S.A. Brawer, and W.B. White, *The structure of lead silicate glasses determined by vibrational spectroscopy.* Journal of Materials Science, 1978. **13**(2): p. 268-282.
60. Furukawa, T., S.A. Brawer, and W.B. White, *Raman and Infrared Spectroscopic Studies of the Crystalline Phases in the System Pb_2SiO_4-$PbSiO_3$.* Journal of the American Ceramic Society, 1979. **62**(7-8): p. 351-356.
61. Worrell, C.A. and T. Henshall, *Vibrational spectroscopic studies of some lead silicate glasses.* Journal of Non-Crystalline Solids, 1978. **29**(3): p. 283-299.
62. Zahra, A.M., C.Y. Zahra, and B. Piriou, *DSC and Raman studies of lead borate and lead silicate glasses.* Journal of Non-Crystalline Solids, 1993. **155**(1): p. 45-55.
63. Ohno, H., et al., *Neutron irradiation effects of $PbO-SiO_2$ glasses.* Journal of Nuclear Materials, 1991. **179-181**: p. 473-476.
64. Liu, L., *Infrared spectroscopy on lead silicate glass.* Zeitschrift für Physik B Condensed Matter, 1993. **90**(4): p. 393-399.
65. Tkachev, S.N., M.H. Manghnani, and Q. Williams, *In situ Brillouin Spectroscopy of a Pressure-Induced Apparent Second-Order Transition in a Silicate Glass.* Physical Review Letters, 2005. **95**(5): p. 057402.
66. Huang, L., et al., *Tailoring structure and properties of silica glass aided by computer simulation.* Journal of Materials Research, 2017. **32**(1): p. 174-182.
67. Rouxel, T., et al., *Poisson's Ratio and the Densification of Glass under High Pressure.* Physical Review Letters, 2008. **100**(22): p. 225501.
68. Grammes, T., et al., *Tailoring the mechanical properties of metaluminous aluminosilicate glasses by phosphate incorporation.* Frontiers in Materials, 2020. **7**: p. 115.

69. Svenson, M.N., et al., *Universal behavior of changes in elastic moduli of hot compressed oxide glasses.* Chemical Physics Letters, 2016. **651**: p. 88-91.
70. Zeidler, A., P.S. Salmon, and L.B. Skinner, *Packing and the structural transformations in liquid and amorphous oxides from ambient to extreme conditions.* Proceedings of the National Academy of Sciences, 2014. **111**(28): p. 10045.
71. Rouxel, T., *Elastic Properties and Short-to Medium-Range Order in Glasses.* Journal of the American Ceramic Society, 2007. **90**(10): p. 3019-3039.
72. Østergaard, M.B., et al., *Revisiting the Dependence of Poisson's Ratio on Liquid Fragility and Atomic Packing Density in Oxide Glasses.* Materials, 2019. **12**(15).
73. Martinet, C., et al., *Permanently densified SiO_2 glasses: a structural approach.* Journal of Physics: Condensed Matter, 2015. **27**(32): p. 325401.
74. Williams, Q., M.H. Manghnani, and T. Matsui, *The effect of coordination changes on the bulk moduli of amorphous silicates: The SiO_2-TiO_2 system as a test case.* American Mineralogist, 2019. **104**(5): p. 679-685.
75. Lin, C.-C., et al., *Anionic structure and elasticity of Na_2O–MgO–SiO_2 glasses.* Journal of Non-Crystalline Solids, 2007. **353**(4): p. 413-425.
76. Golubkov, V.V., et al., *Microinhomogeneities of glasses of the system PbO–SiO_2.* The Journal of Chemical Physics, 1999. **110**(10): p. 4897-4906.
77. Zaid, M.H.M., et al., *Influence of heavy metal oxides to the mechanical and radiation shielding properties of borate and silica glass system.* Journal of Materials Research and Technology, 2021. **11**: p. 1322-1330.